THE ROLE OF CELL CYCLE REGULATION IN THE PROGRESSION OF GIANT CELL TUMOR OF BONE

PhD thesis

Máté Előd Maros

Doctoral School of Pathological Sciences

Semmelweis University

Supervisor: Tibor Krenács, Ph.D., D.Sc.

Official reviewers: Gábor Lotz, MD, Ph.D.
Levente Kuthi MD, Ph.D.

Head of the Complex Examination Committee: Miklós Sárdy, MD, PhD.

Members of the Complex Examination Committee: Katalin Borka, MD, Ph.D.
András Vörös, MD, Ph.D.

Budapest

2023

1. Introduction

1.1. Giant cell tumor of bone

In the current, 5th Edition of the WHO classification of soft tissue and bone tumors, giant cell tumor of bone (GCTB) is categorized into the subgroup of osteoclastic giant cell-rich tumors. GCTB is a locally aggressive lesion that causes pathological osteolysis predominantly affecting the epi-metaphyseal bone regions in young adults. It represents 2-9% of primary and ~20% of benign bone tumors. Despite appropriate treatment, GCTB frequently shows local recurrence in 20-50% of the cases, rarely (in 1-4%) it spreads as "metastatic" embolus to the lung or it might even (in 1-10%) undergo malignant transformation (e.g. into osteosarcoma).

Histologically GCTB is characterized by osteoclast-type giant cells (GC) that are admixed with mononuclear cells. The mononuclear cell fraction consists of osteoclast precursors of monocytic/macrophage lineage and spindle-like stromal cells of osteoblastic origin. Stromal cells represent the neoplastic cell fraction that drive the abnormal osteoclastogenesis in GCTB. Stromal cells in >90% of GCTB cases exhibit hallmark mutations in the H3 Histone Family Member 3A (*H3-3A*) gene, dominantly at Gly34. Furthermore, our research group has shown elevated epidermal growth factor receptor (EGFR) expression and deregulated intercellular connections, mainly reduced gap junctions of connexin43 (Cx43) channels in the stromal cell fraction of recurrent and malignant GCTBs.

Osteoclastogenesis and GC formation is driven by stromal cells through the overexpression of (the canonical pathway of) macrophage colony-stimulating factor (M-CSF) and the growth factor receptor activator of nuclear factor kappa-B (NFκB) ligand (RANKL). As a positive feedback loop, this modified tumor microenvironment further attracts myeloid progenitor cells and monocytes to extravasate from blood into the tumor and initiate their transition to macrophages. During this, monocytes, pre-osteoclasts undergo the polarization process and become tissue specific while committing to the macrophage-osteoclast axis. Ultimately, GCs are created by fusion of pre-osteoclasts and osteoclast-committed macrophages. GCs are the main effectors of pathological bone resorption in GCTB primary by enzymes like cathepsin K and matrix metalloproteinase-9 (MMP-9). Consequently, hemorrhages occur frequently in GCTB and are linked to more aggressive phenotypes.

1.2. Cell cycle regulation

Cells have a sensitive window at the early G1-phase (**Figure 1**) called the restriction point to overcome to access the cell cycle. This process is called licensing that involves the heterohexameric ring complex of minichromosome maintenance 2-7 (MCM2-7) proteins. Besides the general proliferation marker Ki67, MCM2-7 complex proteins can also be detected throughout the cycle except in quiescence (G0).

G1-S-phase transition is primarily initiated by D-type cyclins such as cyclin D1 and its complexing partner cyclin-dependent serine-threonine kinase CDK4/6. These drive the G1/S-phase transition by phosphorylating retinoblastoma (Rb) protein. Thus, the inhibitory control of transcription factor E2F is reduced, which promotes the transcription of cyclinE-CDK2, resulting in a positive feedback loop. This can be prevented by cyclin dependent kinase inhibitors (CDKI) selectively targeting CDK4/6 like $p15^{INK4b}$, $p16^{INK4a}$ and by general inhibitors from the CIP/KIP family as $p21^{WAF1}$ and $p27^{KIP1}$ targeting both cyclin D1 and cyclin E-CDK complexes.

During S-phase, the cyclin A-CDK2 complex mediates transcriptional control of DNA synthesis and drives S/G2-phase transition, whilst topoisomerase 2a (Topo 2a) mediates post-G1-phase DNA cleavage and reassembly. In late G2-phase, cyclin A also binds to CDK1 and promotes G2/M-phase transition. Concurrently, the DNA replication repressor geminin prevents the re-licensing in post-G1-phase through binding to CDT1 (chromatin licensing and DNA replication factor 1) and thereby, blocking the re-loading of the MCM2-7 complex onto chromatin.

During M-phase, the cyclin B1-CDK1 complex catalyzes mitotic cell division by activating the microtubule assembly, chromatin and DNA relaxation for increased gene transcription through the phosphorylation of H1 and H3 histones (pHH3). Concurrently, the G2- and M-phase-related aurora kinase A (AURKA), the “polar kinase”, facilitates the mitotic division by stabilizing the centrosome through associating with the mitotic poles and adjacent spindle microtubules in ana- and telophases. Checkpoint failures during mitosis can cause chromosomal instability and incorrect cytokinesis resulting in poly- or aneuploidy.

The “genomic guardian”, p53, plays a crucial role, as a key tumor suppressor, in preventing aneuploidy through G1 cell cycle arrest by either activating DNA damage response genes or inducing programmed cell death. As a p53 target, cyclin G1 has dual

functions as it can facilitate both cell cycle arrest and S-G2-M progression. For the latter, cyclin G1 might activate the MDM2 oncoprotein by recruiting Ser/Thr protein phosphatase 2A (PP2A), which dephosphorylates MDM2 to inhibit and degrade p53. The p53 with the contribution of $p21^{WAF1}$ can also drive G1 arrest even further to result in cellular senescence.

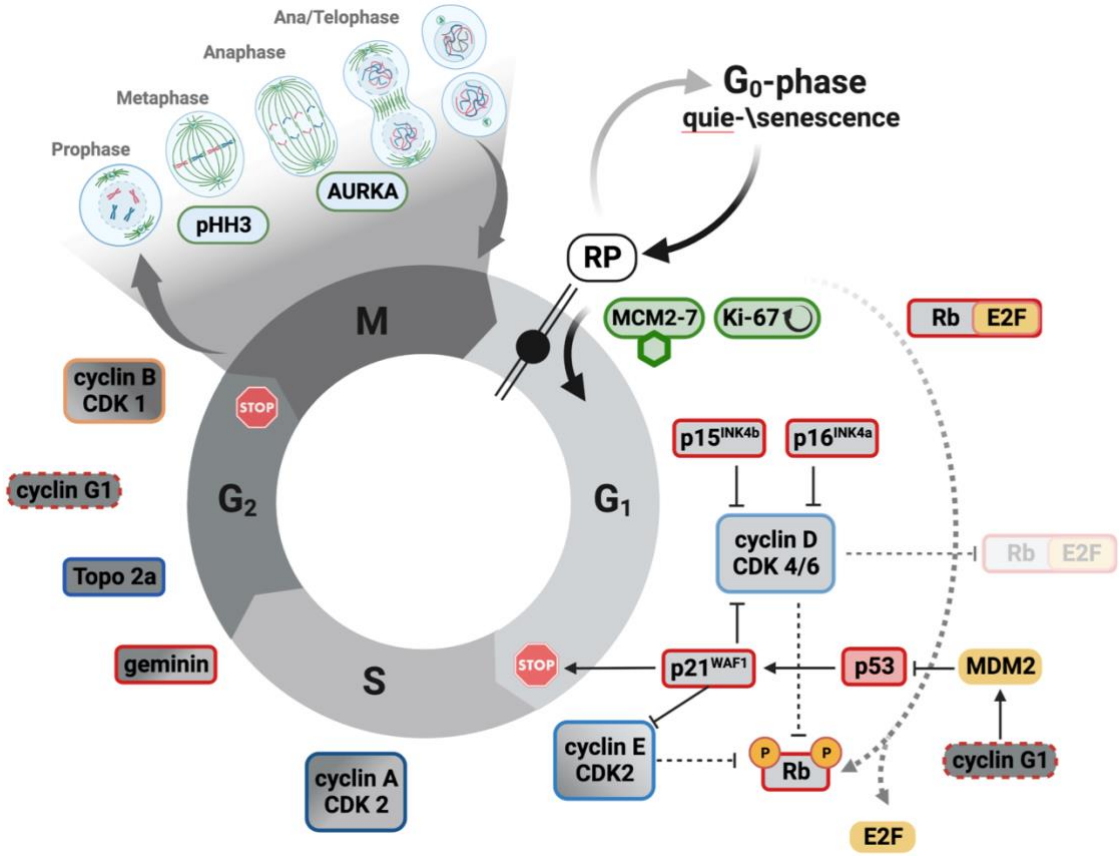

Figure 1. Overview of the cell cycle machinery and the investigated regulatory proteins. Arrows indicate activating- while "T" signs represent inhibitory functions. Stop signs signal the G1/S and G2/M checkpoints. RP (double line with dot) marks the restriction point. The image was created with BioRender.com.

Elevated cell proliferation has already been linked to GCTB progression, but so far only small patient cohorts with limited marker sets focusing on early phases of the cycle have been investigated. A more comprehensive approach including cell cycle control proteins of licensing and late-phase (S-G2-M) promoters had been lacking. Furthermore, the association between mononuclear cell fractions and survival in GCTB has not yet been properly investigated before.

2. Objectives

The doctoral thesis project had the following objectives to study:

1. If cycle regulation has any major defects in the mononuclear cell fraction.
2. If cell cycle fractions in the mononuclear cell compartment can help predict the clinical prognosis of GCTB using progression-free survival (PFS).
3. To properly model PFS in patients with repeated recurrences.
4. To propose a potential prognostic marker set to identify high-risk patients for closer follow-up.
5. If cell cycle regulation can be linked to GC formation.
6. If nuclear cell cycle profile of GCs is associated with lytic activity and osteodestruction (grade).
7. If it is possible to predict the clinical phenotype (primary vs. recurrent) of GCTB cases based on the cell cycle profile of GCs.

3. Materials and methods

3.1. Study cohort

We performed a single-center retrospective cohort study within the EuroBonet network using 154 distinct formalin-fixed and paraffin-embedded surgical cases from 139 GCTB patients, who were diagnosed and operated between 1994-2005 at Institute of Rizzoli, Bologna (IOR), Italy. The studies were approved by the ethical review boards for human research at both the Semmelweis University, Budapest, Hungary (approval nr.: 87/2007) and at the IOR (approval nr.: 13351/5-28-2008) and were performed in accordance with the Declaration of Helsinki. The study focusing on the mononuclear cell fraction included all 154 surgical cases of 100 primary (P), 37 first- (1-Rec), 16 second-/or higher recurrences (2-Rec/3-Rec) GCTBs and one metastasis. For the systematic analysis of GCs, a stratified random sample of 10-10 P and 1-Rec distinct cases was generated from the above cohort.

3.2. Tissue microarray (TMA)

Tissue microarrays (TMA) blocks were created from the archived 154 surgical tissue samples using a 10 x 7 grid pattern of 2 mm diameter tissue cores. Altogether, four TMA blocks were analyzed, which contained 215 TMA tissue cores including duplicates from 56 surgical cases (112), triplicate from a single case (3) and a single core from each of the remaining 100 surgical cases. Of these, 4 μm thick sections were cut and brought onto dewaxed slides.

3.3. Immunohistochemistry (IHC)

Immunostainings of cell cycle proteins were performed on sections cut from TMA blocks. Mouse or rabbit monoclonal primary antibody clones were incubated overnight (~16h) at room temperature including anti-Ki67 Mib1, -B56, -SP6, -MCM2, -MCM6, -CDK2, -CDK4, -cyclin D1, -cyclin E, -cyclin G, -cyclin A, topoisomerase 2, -aurora kinase A, -pHH3Ser10, -p53, -retinoblastoma, -$p15^{INK4b}$, -$p16^{INK4a}$, -$p21^{WAF1}$ and also rabbit polyclonal immunoglobulins for -geminin, -p53 and -retinoblastoma. As detection system, the NovoLink polymer peroxidase kit (Leica-NovoCastra) was used. Immunoreactions were revealed by using diaminobenzidine (DAB Quatro kit, Thermo-Fisher). For double labelling DAB-peroxidase reactions were combined with 3-amino-9-

ethylcarbazole (AEC)-peroxidase reactions. The sections were counterstained with hematoxylin. For double immunofluorescence (mouse Ki67 Mib1; rabbit cyclin D1 and cyclin A) antibodies, were detected simultaneously using Alexa Fluor 488 (green) goat anti-mouse IgG and Alexa Fluor 564 (red) goat anti-rabbit IgG.

3.4. DNA flow cytometry

DNA content measurement was performed using flow-cytometry at the IOR, Italy. For this, nuclear suspension of trimmed cryopreserved GCTB tissue was evaluated using BD Cycletest Plus DNA Kit (BD Biosciences, San Jose, CA, USA). Two thousand cell nuclei per surgical case were measured using BD fluorescence-activated cell sorting (FACS) scan and analyzed in the BD CellFit™ software. DNA content was quantified by the DNA index (DI), which was calculated as the ratio of G0/G1 peaks of cell populations in GCTB specimens compared to the reference of normal bone marrow samples. Diploid and poly-/aneuploid cases were defined as DI=1 or DI≠1, respectively.

3.5. Digital microscopy and image analysis

3.5.1. Mononuclear cells

The immunostained TMA sections were digitalized using a Pannoramic Scan II System and analyzed using its CaseViewer software (both 3DHISTECH, Budapest, Hungary). For the mononuclear cell fraction, each cell cycle marker was manually evaluated by three independent blinded readers in three different GC rich high-power fields (HPF, 40x) of each of the 215 TMA cores. They counted the proportion (%) of the nuclear reactions in marker positive mononuclear cells in relation to all mononuclear cells. Then, a distinct cut-off threshold was set for each marker by averaging the results among readers and converting it to a four-point Likert scale (minimal 0, low 1, medium 2, high 3 proportion). In case of discrepant Likert-scores of dupli- or triplicate parallel TMA cores, the highest value was taken during statistical analyses.

3.5.2. Giant cells

For GCs, the number of GCs (N_{GC}), number of GC nuclei (N_{GC_nuclei}), and respective cell cycle marker positive GC nuclei ($N_{GC\_nuclei+}$) were counted in three GC rich regions of interest (ROI) at HPF 80x per TMA core in the random subcohort of 20 surgical cases

while N_{GC} and N_{GC_nuclei} were additionally averaged over all cell cycle markers for each surgical case for more robust estimates. Furthermore, the ratio for each staining ($N_{GC\_nuclei+}/N_{GC\_nuclei}$) were also calculated to allow for more stable and direct comparisons across cell cycle markers.

3.6. Statistical analyses

We performed exploratory statistical analyses in the R (v.3.6.3, Vienna, Austria) and SAS (v.9.4, Cary, NC, USA) statistics programs. The primary endpoint of the study concerning the mononuclear cell fraction was progression-free survival (PFS) defined as follows: recurrence, local- or distant metastasis, malignant transformation, or death of any cause, which made up a total of 40 progression events during follow-up.

For the first time, Prentice-Williams-Peterson gap time models (PWP-GT) were used for time-to-event analyses in GCTB, which can account for multiple events per patient. Scoring values of cell cycle markers were dichotomized at their medians to produce balanced groups. Both uni- and multivariate PWP-GT models were evaluated, testing all possible combinations up to 5 variables (cell cycle markers and clinical variables) for the latter using automated variable selection based on the Akaike Information Criterion (AIC). Additionally, interaction models and sensitivity analyses as well as Spearman's rank correlation-based unsupervised clustering were also evaluated.

For GCs, the Jonckheere–Terpstra test was used to investigate the overall difference between Enneking's/Campanacci's grading (i.e. latent, active and aggressive), GC count and GC nuclear positivity. As post hoc test, nonparametric Wilcoxon-Mann-Whitney U tests were applied to compare the mean rank of N_{GC}, N_{GC_nuclei}, and $N_{GC\_nuclei+}$ as well as their ratios ($N_{GC\_nuclei+}/N_{GC\_nuclei}$) between P and 1-Rec samples. P-values were adjusted for multiple testing to counteract type 1 error inflation using the conservative Bonferroni correction. Adjusted p-values (p^*) <0.05 were considered significant.

4. Results

4.1. Mononuclear cell fraction

4.1.1. Correlation-based hierarchical clustering of cell cycle marker expression

Unsupervised hierarchical cluster analysis based on Spearman's rank correlations of the Likert-scoring of cell cycle markers revealed no major defect of cell cycle regulation in mononuclear cells while showing the highest correlations between CDKs and their respective complexing cyclins (CDK2-cyclin A, r_{SP}=0.56) or their inhibitors (cyclin D1-$p21^{WAF1}$, r_{SP} =0.51).

4.1.2. Univariate progression-free survival analyses

Univariate PWP-GT models revealed that poly-/aneuploid (HR=5.33, 95%CI: 3.52-8.07, p<0.0001) vs. diploid chromosome set and elevated positive mononuclear cell fractions of cyclin A (HR=2.84, 95%CI: 2.07-3.89, p<0.001), geminin (HR=2.48, 95%CI: 1.70-3.61, p=0.015), MCM2 (HR=3.44, 95%CI: 2.06-5.73, p=0.016) and cyclin D1 (HR=2.20, 95%CI: 1.56-3.10, p=0.022) had significant negative associations with PFS.

4.1.3. Multivariable model selection for progression-free survival analysis

4.1.3.1. Standard multivariable survival models

The AIC-based best multivariate prognostic model (AIC=271.6) and included poly-/aneuploidy (HR=6.20, 95%CI: 2.89-13.30, p<0.0001), cyclin D1 (HR=2.27, 95%CI: 1.10-4.71, p=0.027) and MCM2 (HR=2.64, 95%CI: 0.86-8.08, p=0.090) while the second-best model additionally included cyclin A.

4.1.3.2. Interaction models

We also tested all possible interactions between biomarkers to check whether their association with PFS would stay consistent across different scoring levels. The highest-ranked interaction model (AIC=269.5) was the same as the second-best standard model and included poly-/aneuploidy (p<0.0001), MCM2 (p=0.61), cyclin D1 (p=0.11) and cyclin A (p<0.0001) with a significant interaction between cyclin A and MCM2 (p<0.0001). Furthermore, stratifying GCTB cases based on their mononuclear cell cycle phenotypes showed progressively increasing hazards of reduced PFS for elevated cell cycle commitment and abnormal chromosome numbers.

4.1.2.3. Sensitivity analyses

Despite the multi-rater, independent blinded scoring, only four surgical cases (2.6%) could be identified with incongruent (i.e. cyclin A positive, yet licensing MCM2 negative) staining profiles. After excluding these cases and repeating all previous uni- and multivariate PWP-GT models, we found no relevant interaction regardless of the model building strategy.

4.2. Multinucleated giant cells

4.2.1. Nuclear characteristics of giant cells

Neither the overall average GC number (N_{GC}; p=0.53) nor the average number of GC nuclei (N_{GC_nuclei}; p=0.97) showed statistical difference between P and 1-Rec cases. There was a non-significant trend of inverse association between radiological grade (latent: L; active: A; aggressive: Ag) of GCTB and N_{GC} ($p_{L\_vs\_Ag}$=0.065; $p_{A\_vs\_Ag}$=0.11) and N_{GC_nuclei} ($p_{L\_vs\_A}$=0.093).

4.2.2. Licensing and general proliferation markers in giant cells

Though Ki67 Mib1 positive nuclei in GCs were substantially higher (p=0.012) in 1-Rec than in P cases, it did not reach statistical significance after adjusting for multiple testing ($p^*_{threshold}$=0.0036). Still, the increased average number of Ki67 Mib1 positive nuclei (HR=1.1, 95%CI: 1-1.2, $p_{non\text{-}adj.}$=0.041) was associated with shorter PFS during univariate Cox proportional hazards analyses. None of the other licensing and general proliferation markers showed a relevant difference.

4.2.3. G1/S-phase progression markers in giant cells

The intensity of IHC reactions and the rate of cyclin D1 positive nuclei showed a clear inverse association with signs of aging (larger GCs with higher nuclear density). Nonetheless, nuclear positivity ratios of CDK4 (p=0.72) and cyclin D1 (p=0.25) did not differ statistically in P vs. 1-Rec cases. Similarly, CDK2 was rarely (<8%) detected in GCs (p=0.10). In contrast, cyclin G1 showed extensive (medians >95%) moderate reactions in GC nuclei with a weak, non-significant trend (p=0.091) towards P cases indicating its involvement in cell cycle arrest or rebound upregulation to control p53 overexpression.

4.2.4. Post-G1-phase markers in giant cells

Cyclin A was seldom (<1%) detected in GCs but more likely in mononuclear cells and occasionally in fusing pre-osteoclasts. Geminin was seen only at very low frequency (0-6%), although it appeared more often in 1-Rec cases (p=0.045, n.s.). No other G2-M phase markers (topoisomerase 2a, AURKA and pHH3) could be detected in GC nuclei.

4.2.5. Cell cycle inhibitors in giant cells

Corresponding to increased G1-S nuclear positivity, all CDK inhibitors were detected widely in GC nuclei. However, when systematically analyzed none of the CDKI including $p15^{INK4b}$ (p=1.0), $p16^{INK4a}$ (p=0.69) and $p21^{WAF1}$ (p=0.31) showed differential expression between P and 1-Rec cases. $p16^{INK4a}$ showed the least nuclear positivity but showed widespread cytoplasmic reactions, which might indicate p16-related cellular senescence required for secretory GC activity. In contrast, $p21^{WAF1}$ was strongly detected in most GC nuclei, suggesting its role in p53-induced cell cycle arrest as the main effector.

5. Original findings of the thesis

Our results led to the following original observations:

1. Using a comprehensive set of markers covering the cell cycle machinery, we found no major defect of regulation in the mononuclear cell fraction including the neoplastic stromal cells.
2. We identified a marker panel including poly-/aneuploidy and elevated replication licensing (MCM2), G1-phase (cyclin D1) and S-G2-M-phase (cyclin A) markers while properly modeling subsequent progression events using PWP survival models, which can assist in identifying GCTB patients with increased hazard of progression.
3. Cell cycle-based phenotyping of GCTB cases using this panel was feasible and showed that accelerated cycle in the mononuclear cell fraction (S-G2-M) was increasingly proportional with shorter PFS, in particular in the presence of poly-/aneuploidy.
4. In multinucleated GCs, we demonstrated an early (G1-S-phase) replication activity by the general upregulation of early pro-proliferative markers MCM6, CDK4 and cyclin E, coupled with the widespread, age-dependent expression of cyclin D1.
5. This early G1-S activity is counteracted by the pervasive expression of CDK inhibitors, primarily by the p53- $p21^{WAF1}$ effector pathway resulting in G1 arrest.
6. We also identified the interplay of p53-cyclin G1 pathways and the role of selective CDK4/6 inhibitors ($p15^{INK4b}$, $p16^{INK4a}$) stabilizing G1 arrest and inducing the consequent state of secretory senescence.
7. This was also confirmed by the missing detection of post-G1 markers (such as cyclin A, geminin, topoisomerase 2a, pHH3 and AURKA).

6. Publication list

6.1. Bibliography of the publications relevant to the dissertation

Sum of impact factors relevant to the dissertation: 10.078.

1. **Maros ME**, Balla P, Micsik T, Sapi Z, Szendroi M, Groden C, Wenz H, Forsyth RG, Picci P, Krenacs T. Cell Cycle Regulatory Protein Expression in Multinucleated Giant Cells of Giant Cell Tumor of Bone: do They Proliferate? Pathology and Oncology Research. 2021;27(94). IF: 2.874.

2. **Maros ME**, Schnaidt S, Balla P, Kelemen Z, Sapi Z, Szendroi M, Laszlo T, Forsyth R, Picci P, Krenacs T. In situ cell cycle analysis in giant cell tumor of bone reveals patients with elevated risk of reduced progression-free survival. Bone. 2019;127:188-98. IF: 4.147.

3. Balla P, **Maros ME**, Barna G, Antal I, Papp G, Sapi Z, Athanasou NA, Benassi MS, Picci P, Krenacs T. Prognostic impact of reduced connexin43 expression and gap junction coupling of neoplastic stromal cells in giant cell tumor of bone. PLoS One. 2015;10(5):e0125316. IF: 3.057.

Impact factors as first author relevant to the dissertation: 7.021.
Impact factors as coauthor relevant to the dissertation: 3.057.

6.2. Bibliography of the publications not directly related to the dissertation

Sum of impact factors not directly related to the dissertation: 135.27.

1. Szekely T, Wichmann B, **Maros ME**, Csizmadia A, Bodor C, Timar B, Krenacs T. (2022) Myelofibrosis progression grading based on type-I and type-III collagen and fibrillin-1 expression boosted by whole slide image analysis. Histopathology, doi:10.1111/his.14846. IF: 7.778[#]. [#]expected impact factor.

2. Leinert JL, Weis M, **Maros ME**, Flachsenhaar C, Kosubek M, Durken M. (2022) Scurvy in a Supposedly Healthy 4-Year-Old Picky Eater with Leg Pain and

Refusal to Walk. Klin Padiatr, doi:10.1055/a-1931-3876. IF: 1.236[#]. [#]expected impact factor.

3. Centner F-S, Oster ME, Dally F-J, Sauter-Servaes J, Pelzer T, Schoettler JJ, Hahn B, Fairley A-M, Abdulazim A, Hackenberg KAM, Groden C, Etminan N, Krebs J, Thiel M, Wenz H, **Maros ME**. (2022) Comparative Analyses of the Impact of Different Criteria for Sepsis Diagnosis on Outcome in Patients with Spontaneous Subarachnoid Hemorrhage. Journal of Clinical Medicine, 11: 3873. IF: 4.964[#]. [#]expected impact factor.

4. Kim HE, **Maros ME**, Siegel F, Ganslandt T. Rapid Convolutional Neural Networks for Gram-Stained Image Classification at Inference Time on Mobile Devices: Empirical Study from Transfer Learning to Optimization. In: Biomedicines Vol. 10, 2022. IF: 4.757[#]. [#]expected impact factor.

5. Weyer V, **Maros ME**, Kirschner S, Krost-Reuhl S, Groden C, Kramer M, Brockmann MA, Kronfeld A. (2022) Influence of neurovascular anatomy on perforation site in different mouse strains using the filament perforation model for induction of subarachnoid hemorrhage. PLoS One, 17: e0263983. IF: 3.752[#]. [#]expected impact factor.

6. Kim HE, Cosa-Linan A, Santhanam N, Jannesari M, **Maros ME****, Ganslandt T**. Transfer learning for medical image classification: a literature review. BMC Med Imaging. 2022;22(1):69. IF: 2.795[#]. [#]expected impact factor. **shared last author.

7. Szekely T, Krenacs T, **Maros ME**, Bodor C, Daubner V, Csizmadia A, Vrabely B and Timar B. Correlations Between the Expression of Stromal Cell Activation Related Biomarkers, L-NGFR, Phospho-ERK1-2 and CXCL12, and Primary Myelofibrosis Progression. Pathology and Oncology Research. 2022;28(16):102-17. IF: 2.874[#]. [#]expected impact factor.

8. Kampgen B, Sodmann PF, **Maros ME**, Kluter A. Verstehen was Ärzte schreiben: Kann KI die Datenflut in der Medizin bändigen? (25. fejezet). In: Pfannstiel, M.A. (szerk.) Künstliche Intelligenz im Gesundheitswesen. Springer Gabler, Wiesbaden, 2022:547-564. ISBN 978 3 658 33596 0.

9. Baazaoui H, Hubertus S, **Maros ME**, Mohamed SA, Förster A, Schad LR, et al. Artificial Neural Network-Derived Cerebral Metabolic Rate of Oxygen for Differentiating Glioblastoma and Brain Metastasis in MRI: A Feasibility Study. Applied Sciences. 2021;11(21):9928. IF: 2.838.

10. **Maros ME**, Brekenfeld C, Broocks G, Leischner H, McDonough R, Deb-Chatterji M, Alegiani A, Thomalla G, Fiehler J, Flottmann F, Investigators* GSR. Number of Retrieval Attempts Rather Than Procedure Time Is Associated With Risk of Symptomatic Intracranial Hemorrhage. Stroke. 2021;52(5):1580-8. IF: 10.170.

11. **Maros ME**, Cho CG, Junge AG, Kampgen B, Saase V, Siegel F, Trinkmann F, Ganslandt T, Groden C, Wenz H. Comparative analysis of machine learning algorithms for computer-assisted reporting based on fully automated cross-lingual RadLex mappings. Sci Rep. 2021;11(1):5529. IF: 4.997.

12. Flottmann F, Brekenfeld C, Broocks G, Leischner H, McDonough R, Faizy TD, Deb-Chatterji M, Alegiani A, Thomalla G, Mpotsaris A, Nolte CH, Fiehler J, **Maros ME**, investigators GSR. Good Clinical Outcome Decreases With Number of Retrieval Attempts in Stroke Thrombectomy: Beyond the First-Pass Effect. Stroke. 2021;52(2):482-90. IF: 10.170.

13. Flottmann F, van Horn N, **Maros ME**, McDonough R, Deb-Chatterji M, Alegiani A, Thomalla G, Hanning U, Fiehler J, Brekenfeld C, investigators GSR. Early TICI 2b or Late TICI 3-Is Perfect the Enemy of Good? Clin Neuroradiol. 2021. IF: 3.156[#]. [#]expected impact factor.

14. Flottmann F, van Horn N, **Maros ME**, Leischner H, Bechstein M, Meyer L, Sauer M, Deb-Chatterji M, Alegiani A, Thomalla G, Fiehler J, Brekenfeld C, investigators GSR. More Retrieval Attempts are Associated with Poorer Functional Outcome After Unsuccessful Thrombectomy. Clin Neuroradiol. 2021. IF: 3.156[#]. [#]expected impact factor.

15. Trinkmann F, **Maros M**, Roth K, Hermanns A, Schafer J, Gawlitza J, Saur J, Akin I, Borggrefe M, Herth FJF, Ganslandt T. Multiple breath washout (MBW) testing using sulfur hexafluoride: reference values and influence of anthropometric parameters. Thorax. 2021;76(4):380-6. IF: 9.203.

16. Wichmann B, **Maros ME**, Fabian G, Szász AM. Biostasztika, bioinformatika: A biostatisztika patológiai alkalmazása (18. fejezet). In: Krenacs T, Bodor C, Matolcsy A (szerk.), Patológiai és molekuláris onkodiagnosztikai módszerek: Kézikönyv patológusoknak, kutatóknak, analitikusoknak, asszisztenseknek és a társszakmák képviselőinek. Medicina Könyvkiadó Zrt., Budapest, 2021:591-608. ISBN 978 963 226 767 8.

17. **Maros ME**, Capper D, Jones DTW, Hovestadt V, von Deimling A, Pfister SM, Benner A, Zucknick M, Sill M. Machine learning workflows to estimate class probabilities for precision cancer diagnostics on DNA methylation microarray data. Nat Protoc. 2020;15(2):479-512. IF: 13.491.

18. Westhoff N, Ritter M, **Maros M**, Rassweiler-Seyfried MC, Michel MS, Honeck P, von Hardenberg J. Prospective Feasibility Study of Single-Shot Antibiotic Prophylaxis in Transrectal Focal Ablation of Prostate Cancer. Urol Int. 2020;104(5-6):378-85. IF: 2.089.

19. Weyer V*, **Maros ME***, Kronfeld A, Kirschner S, Groden C, Sommer C, Tanyildizi Y, Kramer M, Brockmann MA. Longitudinal imaging and evaluation of SAH-associated cerebral large artery vasospasm in mice using micro-CT and

angiography. J Cereb Blood Flow Metab. 2020;40(11):2265-77. IF: 6.200. *shared first author.

20. Forster A, Bohme J, **Maros ME**, Brehmer S, Seiz-Rosenhagen M, Hanggi D, Wenz F, Groden C, Pope WB, Giordano FA. Longitudinal MRI findings in patients with newly diagnosed glioblastoma after intraoperative radiotherapy. J Neuroradiol. 2020;47(2):166-73. IF: 3.447.

21. Pino-Lopez L, Wenz H, Bohme J, **Maros M**, Schlichtenbrede F, Groden C, Forster A. Contrast-enhanced fat-suppressed FLAIR for the characterization of leptomeningeal inflammation in optic neuritis. Mult. Scler. J. 2019;25(6):792-800. IF: 5.412.

22. **Maros ME**, Wenz R, Forster A, Froelich MF, Groden C, Sommer WH, Schonberg SO, Henzler T, Wenz H. Objective Comparison Using Guideline-based Query of Conventional Radiological Reports and Structured Reports. In Vivo. 2018;32(4):843-9. IF: 1.609.

23. Forster A*, Wenz R*, **Maros ME***, Bohme J, Al-Zghloul M, Alonso A, Groden C, Wenz H. Anatomical distribution of cerebral microbleeds and intracerebral hemorrhage in vertebrobasilar dolichoectasia. PLoS One. 2018;13(4):e0196149. IF: 2.776. *shared first author.

24. Al-Zghloul M, Wenz H, **Maros M**, Bohme J, Groden C, Forster A. Susceptibility Vessel Sign on T2*-Weighted Gradient Echo Imaging in Lacunar Infarction. In Vivo. 2018;32(4):973-6. IF: 1.609.

25. Wenz H, Wenz R, **Maros M**, Ehrlich G, Al-Zghloul M, Groden C, Forster A. Incidence, Locations, and Longitudinal Course of Cerebral Microbleeds in European Moyamoya. Stroke. 2017;48(2):307-13. IF: 6.239.

26. Gawlitza M, Bohme J, **Maros M**, Lobsien D, Michalski D, Groden C, Hoffmann KT, Forster A. FLAIR vascular hyperintensities and 4D MR angiograms for the estimation of collateral blood flow in anterior cerebral artery ischemia. PLoS One. 2017;12(2):e0172570. IF: 2.766.

27. Wenz H, Wenz R, **Maros ME**, Groden C, Schmieder K, Fontana J. The neglected need for psychological intervention in patients suffering from incidentally discovered intracranial aneurysms. Clin Neurol Neurosurg. 2016;143:65-70. IF: 1.381.

28. Wenz H, **Maros ME**, Meyer M, Gawlitza J, Forster A, Haubenreisser H, Kurth S, Schoenberg SO, Groden C, Henzler T. Intra-individual diagnostic image quality and organ-specific-radiation dose comparison between spiral cCT with iterative image reconstruction and z-axis automated tube current modulation and sequential cCT. Eur J Radiol Open. 2016;3:182-90. IF: NA.

29. Wenz H, **Maros ME**, Meyer M, Forster A, Haubenreisser H, Kurth S, Schoenberg SO, Flohr T, Leidecker C, Groden C, Scharf J, Henzler T. Image Quality of 3rd Generation Spiral Cranial Dual-Source CT in Combination with an Advanced Model Iterative Reconstruction Technique: A Prospective Intra-Individual Comparison Study to Standard Sequential Cranial CT Using Identical Radiation Dose. PLoS One. 2015;10(8):e0136054. IF: 3.057.

30. Wenz H, Kerl HU, **Maros ME**, Wenz R, Kalvin K, Groden C, Nolte I. Signal changes of the alar ligament in a healthy population: a dispositional or degenerative consequence? J Neurosurg-Spine. 2015;23(5):544-50. IF: 2.126.

31. Kirschner S, Felix MC, Hartmann L, Bierbaum M, **Maros ME**, Kerl HU, Wenz F, Glatting G, Kramer M, Giordano FA, Brockmann MA. In vivo micro-CT imaging of untreated and irradiated orthotopic glioblastoma xenografts in mice: capabilities, limitations and a comparison with bioluminescence imaging. J Neuro-oncol. 2015;122(2):245-54. IF: 2.754.

32. Andocs G, Meggyeshazi N, Balogh L, Spisak S, **Maros ME**, Balla P, Kiszner G, Teleki I, Kovago C, Krenacs T. Upregulation of heat shock proteins and the promotion of damage-associated molecular pattern signals in a colorectal cancer model by modulated electrohyperthermia. Cell Stress Chaperones. 2015;20(1):37-46. IF: 2.583.

33. Teleki I, Szasz AM, **Maros ME**, Gyorffy B, Kulka J, Meggyeshazi N, Kiszner G, Balla P, Samu A, Krenacs T. Correlations of differentially expressed gap junction connexins Cx26, Cx30, Cx32, Cx43 and Cx46 with breast cancer progression and prognosis. PLoS One. 2014;9(11):e112541. IF: 3.234.

34. Kiszner G, Wichmann B, Nemeth IB, Varga E, Meggyeshazi N, Teleki I, Balla P, **Maros ME**, Penksza K, Krenacs T. Cell cycle analysis can differentiate thin melanomas from dysplastic nevi and reveals accelerated replication in thick melanomas. Virchows Arch. 2014;464(5):603-12. IF: 2.651.

Impact factors as first- or last author not directly related to the dissertation: 57.172.
Impact factors as coauthor not directly related to the dissertation: 78.098.